Electronic properties of a distorted kagome lattice antiferromagnet $Dy_3Ru_4Al_{12}$

D. I. Gorbunov,[1,2,*] M. S. Henriques,[1,3] A. V. Andreev,[1] A. Gukasov,[4] V. Petříček,[1] N. V. Baranov,[5,6] Y. Skourski,[7] V. Eigner,[1] M. Paukov,[2] J. Prokleška,[2] and A. P. Gonçalves[3]

[1]*Institute of Physics, Academy of Sciences of the Czech Republic, Na Slovance 2, 182 21 Prague, Czech Republic*
[2]*Charles University in Prague, Faculty of Mathematics and Physics, Department of Condensed Matter Physics, Ke Karlovu 5, 121 16 Prague, Czech Republic*
[3]*CCTN, IST/CFMCUL, University of Lisbon, Nuclear and Technological Campus, P-2695-066 Bobadela, Portugal*
[4]*Laboratoire Léon Brillouin, CEA de Saclay, DSM/IRAMIS F-91191 Gif-sur-Yvette, France*
[5]*Institute of Metal Physics, Ural Branch of Russian Academy of Sciences, Kovalevskaya 18, 620990 Ekaterinburg, Russia*
[6]*Institute of Natural Science, Ural Federal University, 620083 Ekaterinburg, Russia*
[7]*Dresden High Magnetic Field Laboratory (HLD), Helmholtz-Zentrum Dresden-Rossendorf, D-01314 Dresden, Germany*

(Received 6 June 2014; revised manuscript received 22 August 2014; published 4 September 2014)

Electronic properties of $Dy_3Ru_4Al_{12}$ (hexagonal crystal structure, Dy atoms form distorted kagome nets) are studied on a single crystal by means of magnetization, neutron diffraction, specific heat, and resistivity measurements. The onset of a long-range magnetic order of Dy moments occurs at 7 K through a first-order phase transition. The compound has a noncollinear antiferromagnetic structure with a propagation vector (1/2 0 1/2). The configuration of the Dy moments is consistent with the monoclinic Shubnikov group C_c2/c. The γ coefficient in the temperature linear term of the specific heat is strongly enhanced to 500 mJ mol^{-1} K^{-2} taking into account the localized nature of Dy magnetism. An additional contribution originates from spin fluctuations induced in the 4*d* subsystem of Ru by the exchange field acting from the Dy 4*f* moments. In an applied magnetic field $Dy_3Ru_4Al_{12}$ displays magnetization jumps along all crystallographic directions. All the metamagnetic transitions are accompanied by large positive magnetoresistance. The maximum effect (125%–140%) is attained for current along the [100] axis and field along the [120] or [001] axes. The large positive effect is explained by changes in the conduction electron spectra through the jumps as the conduction electrons interact with localized magnetic moments.

DOI: 10.1103/PhysRevB.90.094405 PACS number(s): 75.30.Kz, 61.05.F−, 65.40.Ba, 72.15.Gd

I. INTRODUCTION

Solids that contain magnetic ions forming geometrical frustration have in common a triangular arrangement as an elementary object of the structure. In two dimensions, Heisenberg spins on triangular and corner sharing kagome lattices show this effect [1–4], while in three dimensions the most well studied systems are those having a pyrochlore structure, in which the magnetic ions occupy a lattice of corner sharing tetrahedra [1,5–7]. In such systems, a highly degenerate ground state is often favored since it is not possible to satisfy all the interactions. As a result, this geometry frustrates the ordering of the spins and a unique ground state might be selected by a subtle interplay of other weaker perturbations. In some compounds based on rare-earth elements *R* the crucial role is played by the single-ion crystal-field-induced anisotropy [8].

Among intermetallic compounds showing frustration effects, those crystallizing in the hexagonal structure of the ZrNiAl type can be distinguished. In *R*NiAl systems the *R* atoms reside on a crystallographic site that has a triangular symmetry similar to the kagome lattice. The topological frustration reduces the size of the ordered magnetic moments (*R*-Tb) [9–12] or even leads to a paramagnetic state of some magnetic moments in the antiferromagnetically ordered state as found in isostructural CePdAl [13]. The complex balance among all the interactions leads to complicated magnetic structures as found, e.g., in HoNiAl [14] and ErNiAl [15].

Equally interesting physics is found in uranium intermetallic compounds where a geometrical frustration due to the lattice configuration dominates. An example is provided by the $U_3Fe_{4+x}Al_{12-x}$ and $U_3Co_{4+x}Al_{12-x}$ systems having the hexagonal crystal structure of the $Gd_3Ru_4Al_{12}$ type [16–18]. Their magnetism is dominated by uranium whose atoms form a distorted kagome net. As a result of this geometry $U_3Fe_{4+x}Al_{12-x}$ and $U_3Co_{4+x}Al_{12-x}$ enter a spin-glass state at low temperatures. Remarkably, the isostructural compound $U_3Ru_4Al_{12}$ was found to display an antiferromagnetic order with the Néel temperature $T_N = 9.5$ K [19,20]. The uranium magnetic moment was determined to be 2.5 μ_B per atom which is a rather high value for uranium in metallic systems reflecting a high degree of localization of the 5*f* states. Between the basal plane and the hexagonal *c* axis a weak magnetic anisotropy was found, unusual for a uranium intermetallic.

It is known that in uranium intermetallic compounds whose structure has a unique axis (e.g., hexagonal or tetragonal), the U magnetic moments are oriented perpendicular to the shortest U-U links. In $U_3Ru_4Al_{12}$ the shortest interuranium distance, 3.575 Å, occurs within the basal plane (U atoms along the *c* axis are 5.529 Å apart). Contrary to the expectations, the magnetic moments are confined to the basal plane. The formation of the magnetically ordered state and the orientation of the magnetic moments in $U_3Ru_4Al_{12}$ reflect a complex mutual influence of all interactions present in the system.

Since the 5*f* electrons are involved in bonding, understanding of the 5*f* magnetism in $U_3Ru_4Al_{12}$ is complicated. The formation of a magnetic order and its properties can be clarified by studying a magnetic order provided in the same atomic arrangement by fully localized electronic states. To

*Corresponding author: gorbunov@fzu.cz

this end, uranium can be replaced by rare-earth elements with $4f$ electrons. Moreover, $R_3Ru_4Al_{12}$ compounds are themselves interesting objects and deserve special attention despite the interesting physics of $U_3Ru_4Al_{12}$. Several studies were performed on the $R_3Ru_4Al_{12}$ systems with R = La, Ce, Pr, Nd, and Yb where it was demonstrated that the presence of a magnetic order and its type strongly depend on the rare-earth component [21,22]. This finding indicates that exchange interactions and magnetocrystalline anisotropy lift the geometrical frustration, at least partially, and lead to magnetically ordered ground states of $R_3Ru_4Al_{12}$.

The object of the present study is the $Dy_3Ru_4Al_{12}$ compound. Dysprosium was chosen due to its highest magnetic moment ($10\mu_B$ per atom) among the lanthanides and high second-order Stevens factor α_J [23]. α_J describes the asphericity of the $4f$ charge cloud. The shape of the $4f$ orbital and the crystalline electric field determine the magnetocrystalline anisotropy. In this work the ground state of the $Dy_3Ru_4Al_{12}$ compound is determined and its electronic properties studied. It is demonstrated that the electronic state is to a great extent defined by the $4f$ electronic shells. $Dy_3Ru_4Al_{12}$ displays a magnetic order with some fingerprints of geometrical frustration. The latter leads to a complicated noncollinear magnetic structure and a complex behavior of the magnetization and electrical resistivity in magnetic field. Additionally, the electronic effective mass is found to be strongly enhanced by spin fluctuations induced in the Ru $4d$ subsystem by the exchange field acting from the Dy $4f$ shells.

This paper is organized as follows. Upon a presentation of the experimental procedure (Sec. II), the obtained results are reported (Sec. III). This is followed by a discussion and conclusions (Sec. IV).

II. EXPERIMENTAL DETAILS

A $Dy_3Ru_4Al_{12}$ single crystal was grown by a modified Czochralski method in a triarc furnace from a quasistoichiometric mixture of the pure elements (99.9% Dy, 99.99% Ru, and 99.999% Al) having an Al mass excess of 1% on a rotating water cooled copper crucible under protective Ar atmosphere. For the crystal structure determination, a standard powder x-ray diffraction analysis was performed on a part of the single crystal crushed into a fine powder using Cu $K\alpha$ radiation (λ = 1.54184 Å). The diffraction patterns were refined by means of Rietveld analysis using FULLPROF/WINPLOTR software [24]. The compound was found to crystallize in a hexagonal crystal structure of the $Gd_3Ru_4Al_{12}$ type (space group $P6_3/mmc$), isostructural with $U_3Ru_4Al_{12}$ [19,20]. Detailed analyses of this crystal structure are given in Refs. [25–27]. The obtained lattice parameters are a = 8.774 Å and c = 9.530 Å. Backscattered Laue patterns were used to check the crystal quality and to orient it along the [100], [120], and [001] axes to cut the samples for the magnetization and resistivity measurements and for a neutron diffraction study.

An isostructural $Y_3Ru_4Al_{12}$ compound was arc melted with nonmagnetic Y to be used as a reference compound for the determination of the electronic and lattice contributions to the specific heat. The obtained lattice parameters are a = 8.783 Å and c = 9.534 Å. Attempts were also made to prepare the $Lu_3Ru_4Al_{12}$ compound with nonmagnetic Lu in poly- and single-crystalline form, but the resulting samples were not single phase.

Temperature and field variations of the magnetization at T = 2–300 K were measured along the principal crystallographic directions of a 10 mg sample using a standard PPMS-14 magnetometer (Quantum Design) in magnetic fields up to 14 T.

PPMS-14 was also used for specific heat and resistivity measurements. Specific heat in a zero magnetic field was measured by the relaxation method. Temperature and field variations of the electrical resistivity were measured on an oriented sample by the four-contact technique. The excitation current I = 1.5 mA was chosen to flow along either the [100] or the [001] axis.

High-field magnetization curves were measured at T = 2 K in pulsed magnetic fields up to 60 T (pulse duration 20 ms) at the High-Field Laboratory in Dresden-Rossendorf. The magnetization was measured by the induction method using a coaxial pickup coil system. A detailed description of the high-field magnetometer is given in Ref. [28].

A neutron diffraction study was performed at T = 1.5 and 10 K (wavelength λ = 0.9 Å) on a 3 × 3 × 3 mm^3 sample using the Super-6T2 diffractometer at the Orphée reactor of the Laboratoire Léon Brillouin, Saclay, France [29]. First, neutron scattering intensity maps were measured at both temperatures by rotating the sample about the vertical axis with 0.1° step and recording a scattering pattern with an area detector. This procedure allowed us to explore a large three-dimensional (3D) segment of the reciprocal space by transforming a complete set of area detector images in the crystal reciprocal space. Next, 300 nuclear (89 merged equivalents) and 170 magnetic reflections were collected up to sin θ/λ = 0.69 Å^{-1} at T = 1.5 K in a single detector mode. The nuclear structure was ascertained at T = 1.5 and 10 K. In order to check the structural model, an x-ray diffraction study was performed at the Institute of Physics, Prague, Czech Republic. A single crystal of dimensions 0.6 × 0.3 × 0.2 mm^3 was chosen for the experiment. Crystallographic measurements were carried out at T = 100 K on a four-circle CCD diffractometer Xcalibur, Atlas, Gemini ultra, using Mo $K\alpha$ radiation (λ = 0.71073 Å) with graphite monochromator. The JANA2006 package [30] was used to refine the nuclear structure from the x-ray data and the magnetic structure from the neutron data. The refinement confirmed the correctness of the structural model determined by powder and single-crystal x-ray diffraction. The lattice parameters obtained from the single-crystal x-ray diffraction are a = 8.740(4) Å and c = 9.498(4) Å with the R-factor R_{obs} = 1.91%. Refined atomic positions and atomic displacement parameters (ADP) are presented in Table I. However, the standard deviation yielded by the nuclear reflections collected by neutron radiation was relatively large and led us to use the more accurate model as refined from x-ray diffraction with isotropic ADP fixed to a small value of U_{iso} = 0.001 Å^2 at T = 1.5 K. This gave R_{obs} = 14.27%. One of the reasons for such a high R_{obs} might be that magnetic reflections are much weaker than nuclear reflections (this is best seen in Fig. 6 below). Nevertheless, it does not affect the correctness of the refined magnetic structure since all other tested models led to considerably higher R_{obs}.

TABLE I. Refined atomic parameters for $Dy_3Ru_4Al_{12}$.

Atom	Wyckoff position	x	y	z	U_{eq} (Å^2)
Dy	6*h*	0.19255(3)	0.38509(3)	1/4	0.0041(1)
Ru1	6*g*	0.5	0	0	0.0040(2)
Ru2	2*a*	0	0	0	0.0034(2)
Al1	12*k*	0.1625(1)	0.3249(1)	0.5761(2)	0.0051(6)
Al2	6*h*	0.5614(2)	0.1228(2)	1/4	0.0045(7)
Al3	4*f*	1/3	2/3	0.0152(3)	0.0052(6)
Al4	2*b*	0	0	1/4	0.0049(8)

III. RESULTS AND DISCUSSION

A. Magnetization

The upper panel in Fig. 1 shows the temperature dependence of the magnetization M of the $Dy_3Ru_4Al_{12}$ single crystal measured along the principal crystallographic directions in a field of 1 T. A sharp growth of the magnetization is observed below 100 K. It displays an anisotropic behavior with higher values along the [001] axis than those along the basal plane directions. This agrees with the fact that the largest projection of the Dy magnetic moments is along the [001] axis (Fig. 8). The inset in Fig. 1 presents the $M(T)$ variation in a lower field, 0.1 T, along the [100] axis. These data indicate that a transition from paramagnetic to a magnetically ordered state occurs at $T = 7$ K.

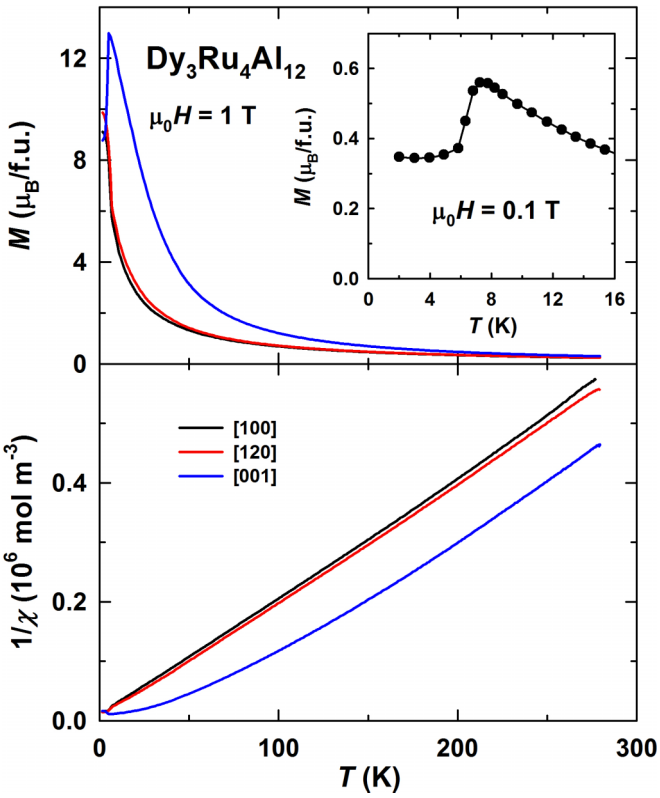

FIG. 1. (Color online) Magnetization (upper panel) and inverse susceptibility (lower panel) as a function of temperature along the [100], [120], and [001] axes of the $Dy_3Ru_4Al_{12}$ single crystal in a field of 1 T. The inset shows the magnetization along the [100] axis in a field of 0.1 T in the vicinity of $T_N = 7$ K.

TABLE II. Effective magnetic moment per Dy atom and paramagnetic Curie temperatures along the [100], [120], and [001] axes of $Dy_3Ru_4Al_{12}$ obtained from fittings using Eq. (1) in the indicated temperatures regions.

	[100]	[120]	[001]
μ_{eff}, μ_B/Dy	10.1	10.2	10.1
θ_p, K	3	4	56
Temperature range (K)	100–300	100–300	170–300

The lower panel in Fig. 1 shows the temperature dependence of the inverse susceptibility χ^{-1}. In the high temperature range the $\chi^{-1}(T)$ functions follow the modified Curie-Weiss law

$$\chi = \frac{C}{T - \theta_p} + \chi_0, \quad (1)$$

where C is the Curie constant proportional to the effective magnetic moment μ_{eff}, θ_p is the paramagnetic Curie temperature, and χ_0 is the temperature-independent term. The values of μ_{eff} per Dy atom and of θ_p are listed in Table II for the [100], [120], and [001] axes (χ_0 was found to be 10^{-8} m^3 mol^{-1} for all directions). The effective Dy magnetic moments are slightly lower than the theoretical value $g_J\sqrt{J(J+1)} = 10.63\mu_B$. Although this might be explained by the presence of extraneous phases, our powder and single-crystal x-ray diffraction did not allow us to detect them within the accuracy provided by the method. The low μ_{eff} should therefore reflect specific interactions that involve the Dy 4*f* electrons, such as crystal-field effects. The reduced values of μ_{eff} may be attributed to the low measuring temperatures in comparison with the total splitting of the energy levels of Dy^{3+} in the strong crystal field. The θ_p values are practically the same for the two axes within the basal plane of the hexagonal lattice. However, the difference between the paramagnetic Curie temperatures between the basal plane and the [001] axis is high, which reflects a strong anisotropy of magnetic properties between them. Deviations from the Curie-Weiss behavior appear already below 170 K, which indicates the persistence of spin correlations above magnetic ordering temperature.

Magnetization curves along the [100], [120], and [001] axes of the $Dy_3Ru_4Al_{12}$ single crystal at $T = 2$ K are presented in Fig. 2. The spontaneous magnetic moment is zero along all the directions, which means that the compound is an antiferromagnet. $Dy_3Ru_4Al_{12}$ displays a complicated behavior in a magnetic field manifested by field-induced magnetic phase transitions: one along [100], two along [120], and two along [001]. First, the magnetization experiences a jump at the critical field 0.9 T along the [100] and [120] axes and at 0.4 T along the [001] axis (the critical fields of the transitions were determined as the average field between their ascending and descending branches). With a further field increase, an additional transition is observed along the [001] axis at 1.2 T and at a much higher field, 7 T, along the [120] axis. The magnetization value which corresponds to the ferrimagneticlike state observed after the first metamagnetic transition along the [001] direction is about one-third ($\sim 8\mu_B$/f.u.) of the saturation value. All the transitions exhibit hysteresis and are of first order. Above the transitions the magnetization continues to grow as the magnetic moments continue to rotate. In this field

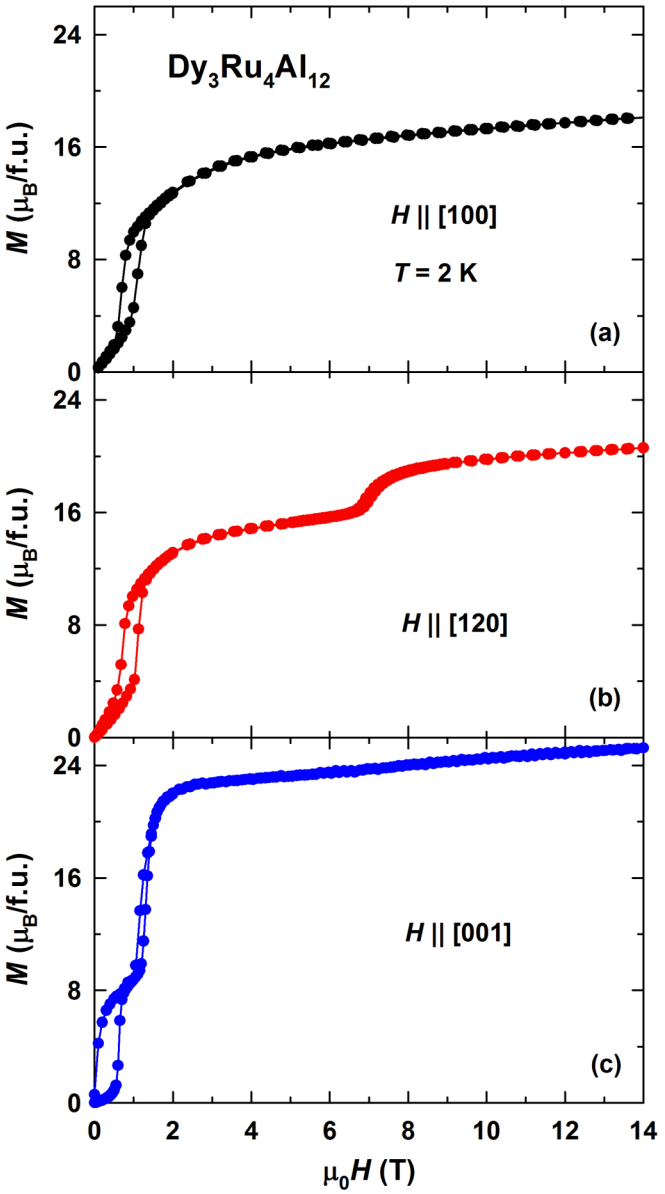

FIG. 2. (Color online) Magnetization curves along the [100] (a), [120] (b), and [001] (c) axes of the $Dy_3Ru_4Al_{12}$ single crystal at $T = 2$ K.

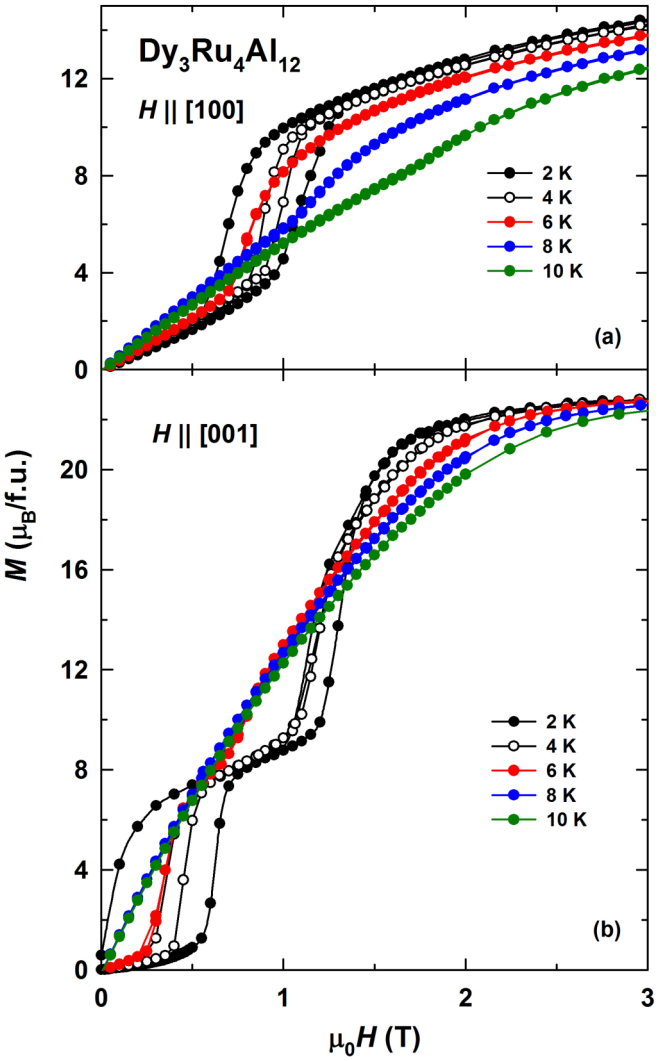

FIG. 3. (Color online) Temperature evolution of the magnetization curves along the [100] (a) and [001] (b) axes of the $Dy_3Ru_4Al_{12}$ single crystal in the range $T = 2$–10 K.

region the highest magnetization is attained along the [001] axis, $\approx 24\mu_B$/f.u.

The temperature evolution of the magnetization along the [100] and [001] axes in fields up to 3 T is shown in Fig. 3. With increasing temperature the magnetization jumps become more smeared out and finally disappear in the vicinity of the Néel temperature, $T_N = 7$ K. Hysteresis at all magnetization jumps is negligible at $T > 4$ K. The transition fields display practically no temperature dependence below 6 K. The magnetization curve along the [120] axis (not shown) changes with temperature in a similar manner.

The observed field-induced phase transitions reflect rotation of the magnetic moments from the initial antiferromagnetic state to a noncollinear ferromagnetic state. The magnetization of the collinear ferromagnetic state is three times Dy magnetic moment $M_{Dy} = g_J J = 10\,\mu_B$: $M_{ferro} = 3 \times M_{Dy} = 30\mu_B$/f.u. The collinear ferromagnetic state is not reached along any direction in fields up to 14 T.

From the data presented in Figs. 2 and 3 it is clear that $Dy_3Ru_4Al_{12}$ displays strong magnetocrystalline anisotropy. Along the two axes in the basal plane the magnetization is rather close in absolute value, whereas the difference between the basal plane and the [001] axis is much larger. This result correlates well with the θ_p values obtained for the same axes (see Fig. 1 and Table II).

Figure 4 shows an extension of the magnetization curves of $Dy_3Ru_4Al_{12}$ to 60 T. No more magnetization jumps are observed; the magnetization grows monotonously up to the highest available field. The magnetocrystalline anisotropy is seen up to 60 T.

The complex behavior of the magnetization of $Dy_3Ru_4Al_{12}$ reflects an intricate balance among exchange interactions, magnetocrystalline anisotropy, and Zeeman energy. The compound's magnetic structure is expected to be rather complicated. Moreover, it should be noted that, although $Dy_3Ru_4Al_{12}$ is an antiferromagnet, positive paramagnetic

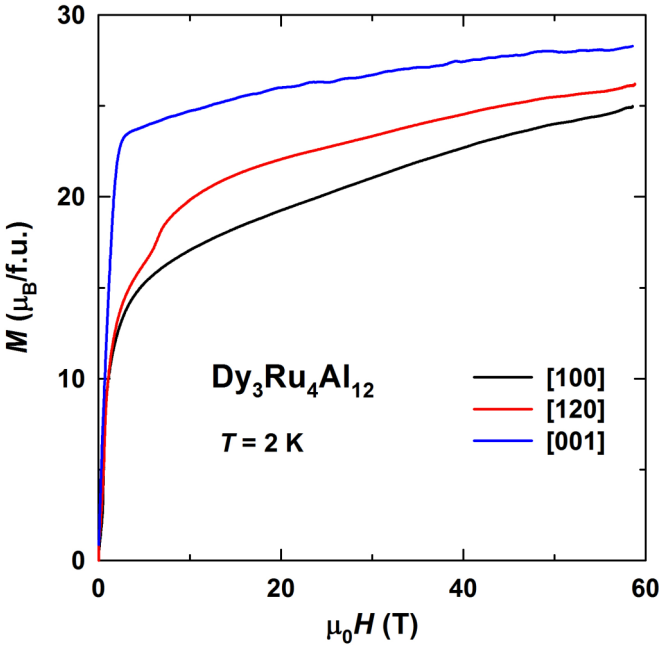

FIG. 4. (Color online) Magnetization curves along the [100], [120], and [001] axes of the $Dy_3Ru_4Al_{12}$ single crystal at $T = 2$ K in pulsed magnetic fields up to 60 T.

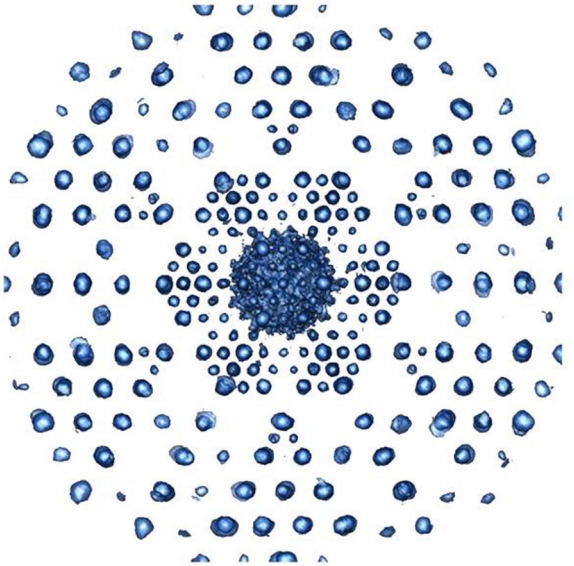

FIG. 5. (Color online) 3D equal intensity surfaces in the reciprocal space of $Dy_3Ru_4Al_{12}$ at $T = 1.5$ K. The reconstructed volume was completed with its symmetrically equivalent orientations employing the Laue symmetry of the structure.

Curie temperatures point to a dominance of ferromagnetic exchange interactions. In order to determine the magnetic structure of the $Dy_3Ru_4Al_{12}$ compound, a single-crystal neutron diffraction study was undertaken.

B. Neutron diffraction

A typical 3D representation of an equal scattering intensity surface at $T = 1.5$ K is shown in Fig. 5. From this pattern, a series of conventional 2D cuts (*hhl*) perpendicular to the [001] axis were extracted, which showed the presence of magnetic satellites with propagation vector $\boldsymbol{k} = (1/2\ 0\ 1/2)$ and its equivalent ones. This can be seen from Fig. 6, where the (*hh*0) and ($h\ h\ 1/2$) cuts are shown. Thus, the magnetic structure of $Dy_3Ru_4Al_{12}$ can be described in a magnetic cell doubled in the a and c directions with respect to the structural unit cell.

The temperature evolution of some magnetic reflections was followed to monitor the transition from the magnetically ordered to the paramagnetic state. Figure 7 presents the temperature variation of the magnetic reflection $(5/2\ -5/2\ 1/2)$. An abrupt decrease of the magnetic intensity occurs around $T = 7$ K, at the Néel temperature of the compound. A similar behavior was observed for other magnetic reflections. No hysteresis was detected in the "order-disorder" transition.

Two solutions of the magnetic structure providing the best fit with the experimental data were obtained within the monoclinic centrosymmetric Shubnikov group C_c2/c. The two corresponding magnetic space groups, C_c2/c and C_c2/c+(0 0 1/4), differ in the origin position. The resulting magnetic structure models cannot be distinguished from the refinements as they both give almost identical R values. The two possible magnetic structures are compared in Fig. 8 with only the Dy atoms displayed for clarity. For this figure we used an orthorhombic unit cell with parameters $a_O = 8.740$ Å,

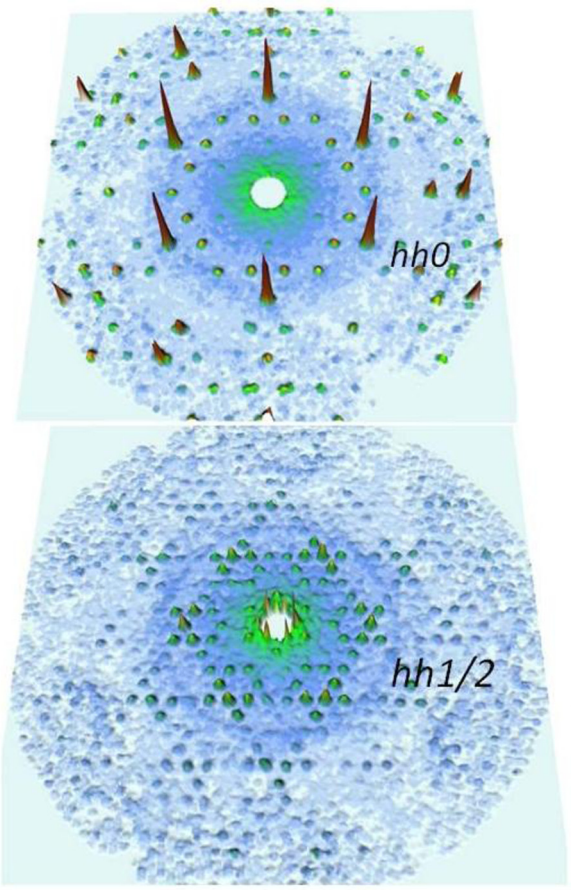

FIG. 6. (Color online) Nuclear reflections in the (*hh*0) plane (top figure) and magnetic satellites in the ($h\ h\ 1/2$) plane (bottom) at $T = 1.5$ K.

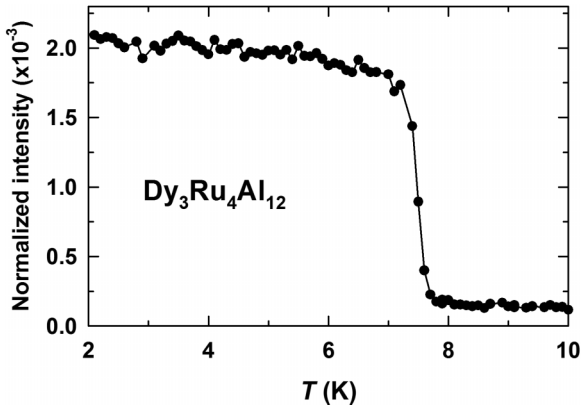

FIG. 7. Temperature dependence of the intensity of the magnetic reflection (5/2 −5/2 1/2).

$b_O = 15.139$ Å, and $c_O = 18.997$ Å related to the original hexagonal basis by the equations $\mathbf{a_O} = \mathbf{a_H}, \mathbf{b_O} = \mathbf{a_H} + \mathbf{2b_H}$, and $\mathbf{c_O} = \mathbf{2c_H}$. This nonstandard setting (the monoclinic axis is oriented along $\mathbf{a_O}$) has been chosen to keep consistency with magnetic measurements. In this setting the magnetic symmetries are alternatively described by the nonstandard Shubnikov symbols I_c2/c and $I_c2/c + (0\,0\,1/4)$.

The magnetic structure of $Dy_3Ru_4Al_{12}$ is noncollinear, with the magnetic moments not confined to any high-symmetry crystallographic directions. Each Dy atom carries an ordered magnetic moment, and the magnetic structure refinement yielded close values of the magnetic moment M_{Dy} at $T = 1.5$ K, nearly $10\mu_B$, for all Dy atoms. As seen from Figs. 8(b) and 8(d), the vertical layers of the Dy atoms lying on the faces of the parallelepiped and the vertical layer in the middle have the magnetic moments confined to the (bc) plane as there is no projection onto the a axis. For the space group C_c2/c [C_c2/c+(0 0 1/4)] these moments form the angle of 50.5° (52°) with the c axis and 39.5° (38°) with the b axis. The magnetic moments of the rest of the Dy atoms do have projections onto the three perpendicular directions. The corresponding components of the magnetic moments make the following angles with the a, b, and c axes: 53.5° (50°), 89° (89°), and 36.5° (40°), respectively. Thus, for both possible magnetic structures the largest component of the Dy magnetic moments is the one projected onto the c axis.

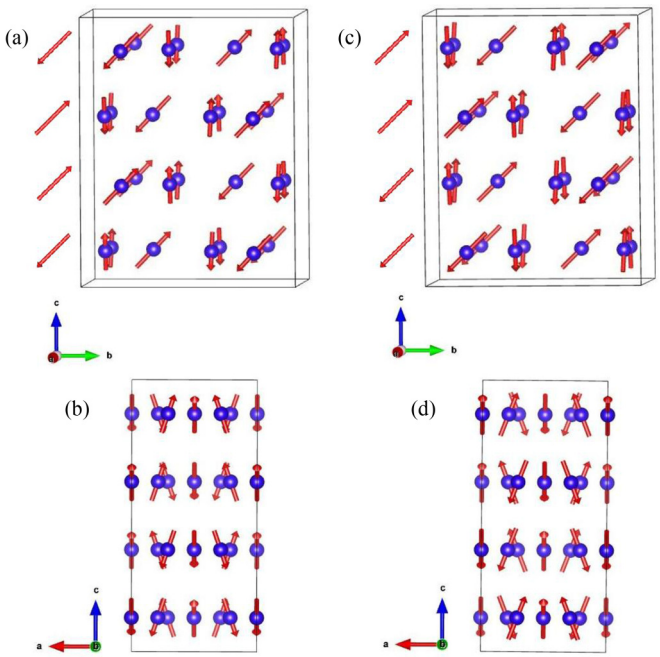

FIG. 8. (Color online) Two possible magnetic structures of the $Dy_3Ru_4Al_{12}$ compound: (a) C_c2/c and (c) $C_c2/c + (0\,0\,1/4)$, and [(b) and (d)] the view of their (ac) plane. The structures are represented within an orthorhombic unit cell. For clarity only the Dy atoms are shown.

In the presented orthorhombic structure four horizontal layers of Dy atoms can also be distinguished. To the left of Figs. 8(a) and 8(c) the net magnetic moments within each layer are shown. In the structure having the symmetry I_c2/c the upper and lower layers give a net ferromagnetic component pointing to the lower left corner of the displayed orthorhombic unit cell. The two layers in the middle give the same ferromagnetic component but it points to the upper right corner. In the structure with the shifted origin, I_c2/c+(0 0 1/4), the same ferromagnetic components are formed by the two upper and two lower layers. Again, they point in the opposite directions. Thus, the net magnetic moment of the whole structure is zero, in accordance with the magnetization data that indicate an antiferromagnetic state of $Dy_3Ru_4Al_{12}$.

A refinement of a magnetic moment on the Ru atoms was also attempted using the same Shubnikov groups. This increased the number of parameters refined from 6 to 30 but no significant improvement of the R factor was detected. This allows us to conclude that the moment of Ru (if any) is less than $0.5\mu_B$, which corresponds to the error bars of our refinement.

C. Specific heat

The temperature dependence of the specific heat C_p of the $Dy_3Ru_4Al_{12}$ single crystal is shown in Fig. 9(a). The sharp maximum at $T_N = 7$ K indicates the phase transition from the antiferromagnetic to the paramagnetic state [see also lower inset in Fig. 9(a)]. In order to study the nature of the transition more thoroughly, the temperature-time relaxation curve was followed for a heat pulse [red curve in Fig. 9(b)] driving the sample above T_N. Both the heating and cooling regimes display plateaus [black curve in Fig. 9(b)] which are a feature of transitions involving latent heat.

The temperature dependence of the specific heat may be described by the expression

$$C_p = C_{el} + C_{ph} + C_{magn} \qquad (2)$$

that represents the electronic $C_{el} = \gamma T$, phonon $C_{ph} = \beta T^3$ [described by Eq. (3) below], and magnetic C_{magn} contributions.

Since the "order-disorder" transition occurs for $Dy_3Ru_4Al_{12}$ at a rather low temperature, the electronic contribution to the specific heat cannot be determined precisely. An approximate value of this parameter, $\gamma(0)$, can be found by extrapolating to zero the linear part of the $C_p/T(T^2)$ function just above the transition [upper inset in Fig. 9(a)]. The thus determined value of $\gamma(0)$ is about 500 mJ mol^{-1} K^{-2}. The strongly enhanced $\gamma(0)$ in comparison with γ for $Y_3Ru_4Al_{12}$, also shown in the upper inset in Fig. 9(a),

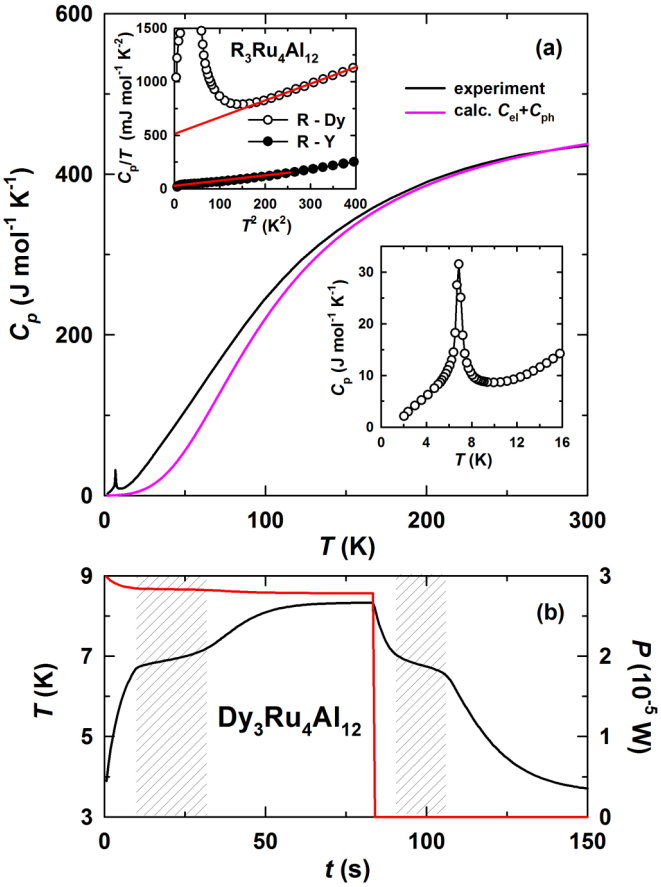

FIG. 9. (Color online) (a) Temperature dependence of the specific heat of $Dy_3Ru_4Al_{12}$: total measured and calculated nonmagnetic part. The lower inset shows the $C_p(T)$ function for $Dy_3Ru_4Al_{12}$, and the upper inset shows the $C_p/T(T^2)$ function for $Y_3Ru_4Al_{12}$ and $Dy_3Ru_4Al_{12}$ in the vicinity of $T_N = 7$ K. (b) The time dependence of power P supplied to the sample (red) and the temperature-time relaxation curve (black) around T_N of $Dy_3Ru_4Al_{12}$. The shaded areas indicate the arrests due to the latent heat at the phase transition.

points to an additional contribution to the T-linear specific heat term. A high $\gamma(0)$ value, $\approx$600 mJ mol^{-1} K^{-2}, was also reported for the U-based compound, $U_3Ru_4Al_{12}$ [20].

In order to explain the effective mass enhancement in $Dy_3Ru_4Al_{12}$, we consider three main mechanisms: (a) electron-phonon interaction, (b) electron-magnon interaction, and (c) spin fluctuations.

In principle, the electron-phonon effects can be excluded as the primary origin of the observed mass enhancement since $Dy_3Ru_4Al_{12}$ and $Y_3Ru_4Al_{12}$ have the same crystal structure with very close values of the lattice parameters, and their molar masses, 1216 and 995 g/mol, respectively, differ by only about 20%. Nevertheless, as the phonon dispersion relation depends on the mass of the vibrating atoms, the mass differences between Y and Dy might give rise to a different contribution to the electron-phonon interaction between the two compounds. The electron-magnon interaction is also very unlikely to lead to the high $\gamma(0)$ value in $Dy_3Ru_4Al_{12}$, as follows from a comparison between the Sommerfeld coefficients of pure Dy and Y: $\gamma = 4.9$ mJ mol^{-1} K^{-2} [31] and $\gamma = 7.9$ mJ mol^{-1} K^{-2} [32], respectively. Since the difference between the two γ values is small, the presence of a magnetic order in Dy does not significantly affect the electronic effective mass in comparison with Y.

The third proposed mechanism takes into account exchange interactions in $Dy_3Ru_4Al_{12}$. The magnetic order in this system is mediated by the indirect $4f$-$4f$ exchange coupling. It is known to proceed via the intra-atomic $4f$-$5d$ and inter-atomic $5d$-$5d$ exchange interactions between spin-polarized $5d$ electrons of neighboring atoms [33]. As regards the $4d$-$4d$ exchange interaction within the Ru sublattice, it should not be sufficiently strong to induce the $4d$-band splitting. However, the exchange field acting from the Dy $4f$ shells may induce magnetic moments and/or spin fluctuations in the Ru $4d$ electron subsystem through the $4f$-$5d$-$4d$-$5d$-$4f$ mechanism and the $4d$-$5d$ hybridization. Therefore, the $4d$ electrons may be involved in the exchange interactions, thus affecting physical properties of $Dy_3Ru_4Al_{12}$ despite the absence or a very low value of the Ru magnetic moment (the neutron diffraction data do not allow us to detect an ordered moment on Ru; see above). The spin fluctuations in the $4d$ electron subsystem should give an additional contribution to the specific heat.

In fact, an enhancement of the electronic effective mass was earlier observed in binary R-Rh and R-Ni compounds [34,35]. In particular, R_3Rh, RNi, and RNi$_2$ systems with nonmagnetic rare-earth elements are paramagnetic (see, e.g., [36–38]). Their γ values are of the order of 10 mJ mol^{-1} K^{-2} [34,35]. The presence of a magnetic rare-earth component stabilizes a magnetic order in these systems. Due to an exchange field acting from the Gd subsystem on the d electron subsystem of Rh the electronic contribution to the specific heat of Gd_3Rh increases by an order of magnitude [34]. In the GdNi and $GdNi_2$ compounds the Ni atoms were found to carry an induced magnetic moment $\sim 0.1\mu_B$ [39–41], and just as strong enhancement of γ was observed [35]. Spin fluctuations induced by the f-d exchange interaction were considered responsible for the additional contribution to the T-linear specific heat.

The magnetic contribution to C_p of $Dy_3Ru_4Al_{12}$ was determined by subtracting the nonmagnetic part, $C_{el} + C_{ph}$, from the total specific heat. For the electronic contribution, $C_{el} = \gamma T$, the value $\gamma = 32$ mJ mol^{-1} K^{-2} for $Y_3Ru_4Al_{12}$ was used [see upper inset in Fig. 9(a)]. In order to calculate the phonon contribution, the Debye function was implemented:

$$C_{ph}(T) = 9Nk_B\left(\frac{T}{\Theta_D}\right)^3 \int_0^{\Theta_D/T} \frac{x^4 e^x}{(e^x-1)^2} dx, \qquad (3)$$

where N is the number of atoms per formula unit ($N = 19$) and Θ_D is the Debye temperature. Although one has to take into consideration that Y has a significantly smaller atomic mass in comparison with Dy, which might account for underestimation of the lattice contribution to the specific heat in the case of $Dy_3Ru_4Al_{12}$, its Debye temperature might be rescaled to better reflect the lattice dynamics. The Θ_D value for $Dy_3Ru_4Al_{12}$ can be derived using its molar mass m and unit cell volume v and those of $Y_3Ru_4Al_{12}$:

$$\frac{\Theta_D(Dy_3Ru_4Al_{12})}{\Theta_D(Y_3Ru_4Al_{12})} = \left[\left(\frac{m_{Y_3Ru_4Al_{12}}}{m_{Dy_3Ru_4Al_{12}}}\right)\left(\frac{v_{Y_3Ru_4Al_{12}}}{v_{Dy_3Ru_4Al_{12}}}\right)^{1/3}\right]^{1/2}. \qquad (4)$$

An assumption behind the validity of this equation is that the binding forces in the $R_3Ru_4Al_{12}$ compounds vary roughly as $v^{-1/3}$. Using $\Theta_D = 476$ K for $Y_3Ru_4Al_{12}$, we obtained $\Theta_D = 431$ K for $Dy_3Ru_4Al_{12}$. The resulting magnetic contribution to the specific heat of $Dy_3Ru_4Al_{12}$ is seen in Fig. 9(a) as the difference between the measured (black) and calculated (pink) curves.

The magnetic entropy gain at the Néel temperature is estimated to be $S_{mag} = 13$ J mol^{-1} K^{-1} for $Dy_3Ru_4Al_{12}$. This value is of course much lower than the expected value, $S_{mag}^{max} = 3R\ \ln(2J+1) = 69$ J mol^{-1} K^{-1} ($J = 15/2$ for Dy). The Kramers character of the Dy^{3+} ion implies a splitting of the $J = 15/2$ ground state multiplet into eight doublets by crystal-field interactions. An internal molecular field or external magnetic field induces a Zeeman splitting of the doublets. If only the lower doublet is involved in the formation of a magnetically ordered state in $Dy_3Ru_4Al_{12}$, the magnetic entropy gain at $T = T_N$ should reach a value of $3R\ \ln(2) = 17.3$ J mol^{-1} K^{-1}. Together with crystal-field effects the huge difference between S_{mag} and S_{mag}^{max} can be attributed to the presence of short-range correlations between Dy moments well above T_N. Moreover, Dy alone cannot account for the total magnetic entropy that is estimated to be 95 J mol^{-1} K^{-1}, higher than S_{mag}^{max}. This suggests an additional contribution to the magnetic entropy which we attribute to Ru, in accordance with the analysis above.

Despite a rather high magnetic moment in $U_3Ru_4Al_{12}$, 2.5 μ_B per U atom, the compound displays a weak λ-type anomaly at $T_N = 9.5$ K [20]. Consequently, the estimated magnetic entropy at the Néel temperature is very low, $S_{mag} = 1.3$ J mol^{-1} K^{-1}. The reason is not clear. For the $Dy_3Ru_4Al_{12}$ compound, being a localized system with an ordered magnetic moment of $10\mu_B$ per Dy atom, S_{mag} at $T = T_N$ is an order of magnitude higher.

D. Electrical resistivity

The temperature dependence of the electrical resistivity $\rho(T)$ of $Dy_3Ru_4Al_{12}$ is presented in Fig. 10 for two current flowing directions, [100] and [001]. At $T = 2$ K the resistivity has typical metallic values not exceeding 30 $\mu\Omega$ cm. The transition into the disordered state is accompanied by an abrupt stepwise increase in the electrical resistivity (see also inset in Fig. 10). Above the transition the $\rho(T)$ curve displays metallic behavior. It can be well described by the Bloch-Grüneisen-Mott expression [42]

$$\rho = \rho_{01} + c\Theta_D\left(\frac{T}{\Theta_D}\right)^5 \times \int_0^{\Theta_D/T} \frac{x^5}{[e^x - 1][1 - e^{-x}]} - KT^3, \quad (5)$$

where ρ_{01} is the resistivity just above the phase transition, the second term (Bloch-Grüneisen formula) represents the scattering of conduction electrons on thermally excited phonons, and the third term describes *s*-*d* interband scattering. The fits are also shown in Fig. 10, and the fitting parameters are given in Table III. The large discrepancy between the Debye temperatures determined for $Dy_3Ru_4Al_{12}$ from specific heat and resistivity measurements should result from limitations of the Bloch-Grüneisen model since it does not consider umklapp processes and allows coupling of electrons with longitudinal phonons only. Furthermore, the existence of other scattering mechanisms cannot be excluded.

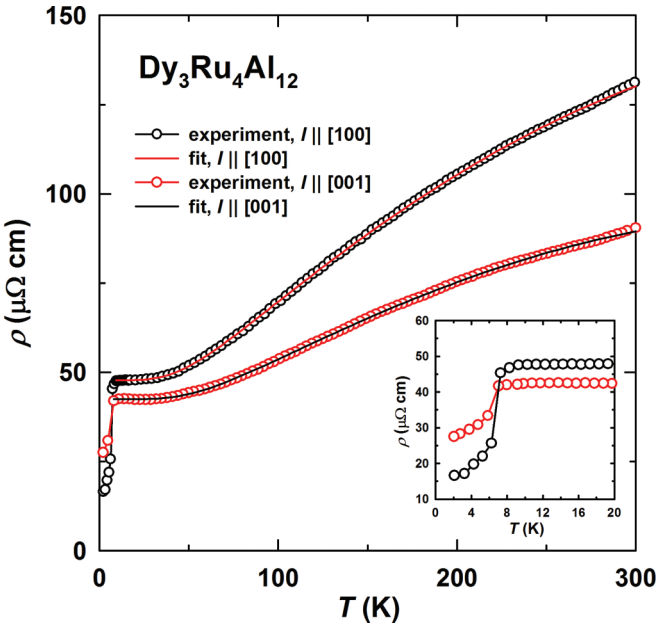

FIG. 10. (Color online) Temperature dependence of the electrical resistivity of $Dy_3Ru_4Al_{12}$. The inset shows the $\rho(T)$ functions in the vicinity of $T_N = 7$ K.

E. Magnetoresistance

Figure 11 shows longitudinal and transverse magnetoresistance $\Delta\rho/\rho$ of the $Dy_3Ru_4Al_{12}$ single crystal. The majority of the field-induced magnetization jumps (see also Fig. 2) are accompanied by large positive magnetoresistance. The effects are much larger for $I \parallel [100]$ ($\Delta\rho/\rho \sim 80\%$ in the longitudinal and ~125%–140% in the transverse geometry) than for $I \parallel [001]$ ($\Delta\rho/\rho \sim 50\%$ in both geometries). For both current directions, at the low-field transitions the magnetoresistance is smaller in the longitudinal than in the transverse geometry. It is also interesting to note that the second field-induced transition along the [120] direction that occurs at 7 T is not seen on the $\Delta\rho/\rho(H)$ curves. It leads us to assume that at this transition the magnetic structure of the compound undergoes relatively small changes in comparison with the other transitions, which is supported by a much smaller magnetization jump, ~2.5 μ_B/f.u. Much smaller magnetoresistance was reported for $U_3Ru_4Al_{12}$ [20]. Large positive magnetoresistance was also observed in other antiferromagnetic compounds RGa_2 (R-Ho, Dy) ($\Delta\rho/\rho$ up to 70% [43]) and R_5Si_3 (R-Tb,

TABLE III. Parameters used to fit the $R(T)$ curves (Fig. 10) according to Eq. (5).

	ρ_{01} ($\mu\Omega$ cm)	c ($\mu\Omega$ cm K^{-1})	Θ_D (K)	K (10^7 $\mu\Omega$ cm K^{-3})
$I \parallel [100]$	48	1.42	294	7
$I \parallel [001]$	42	0.85	341	4.4

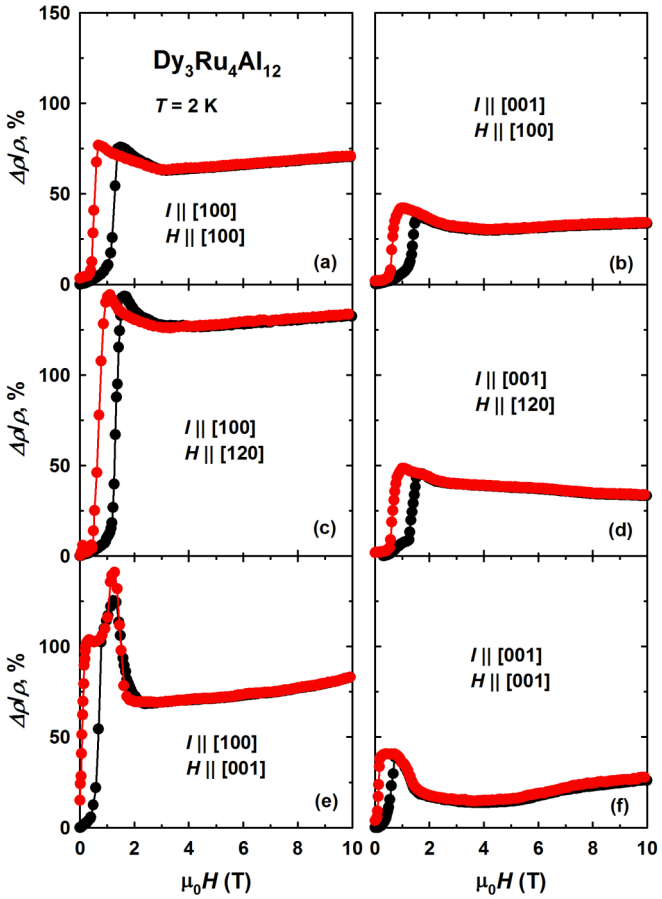

FIG. 11. (Color online) Magnetoresistance of the $Dy_3Ru_4Al_{12}$ single crystal in the longitudinal and transverse geometries at $T = 2$ K. The black and red curves represent the data obtained in ascending and descending fields, respectively.

Er) ($\Delta\rho/\rho \sim 70\%-160\%$ [44,45]) with hexagonal crystal structures.

In $Dy_3Ru_4Al_{12}$, there are two field intervals with different magnetoresistance behaviors: (i) $0 < \mu_0 H < 2$ T where the magnetoresistance shows drastic changes in the vicinity of the field-induced phase transitions and (ii) $\mu_0 H > 2$ T where the sample is in the field-induced states with high magnetization values. Usually, antiferromagnetic-ferromagnetic phase transitions under application of a magnetic field are accompanied by a reduction of the resistivity owing to the disappearance of superzones and energy gaps on superzone boundaries since, as shown by Elliot and Wedgwood [46], the superzones result in an increased resistivity of antiferromagnets. However, the magnetic states induced in $Dy_3Ru_4Al_{12}$ by application of a magnetic field above 2 T cannot be considered as simple ferromagnetic ones because the magnetization values do not reach the expected value $30\mu_B$/f.u. (see Fig. 2). Therefore, one can suggest that the application of a magnetic field along the main crystallographic directions of the $Dy_3Ru_4Al_{12}$ single crystal induces phase transitions to magnetic states with incommensurate magnetic structures having ferromagnetic components along the field direction and a different periodicity in comparison with the initial zero-field magnetic structure. Such transitions may be accompanied by a positive magnetoresistance. The possibility of the appearance of incommensurate magnetic phases at low temperatures under application of a magnetic field with a longer periodicity was inferred by Gignoux and Schmitt [47] from the consideration of a mean-field model which takes into account the periodic exchange field and crystal-field effects. It is worth noting that the $Dy_3Ru_4Al_{12}$ single crystal in a ferrimagneticlike state above the first metamagnetic transition along the [001] axis exhibits an increased resistivity [see Figs. 11(e) and 11(f)] in comparison with the initial noninfluenced state and with the forced magnetic state with ferromagnetic components ($\mu_0 H > 2$ T). Neutron diffraction measurements in magnetic fields applied along different crystallographic directions are strongly desirable to verify the assumption about the appearance of field-induced incommensurate magnetic structures in $Dy_3Ru_4Al_{12}$.

The $\Delta\rho/\rho(H)$ curves of $Dy_3Ru_4Al_{12}$ in the first field interval ($0 < \mu_0 H < 2$ T) are characterized by resistivity peaks in the vicinity of the field-induced magnetic transitions. In these field regions there exist domains with different magnetic structures, and the compound is in a thermodynamically stable intermediate state (see, e.g., [48]). There are two main reasons for an additional contribution to the electrical resistivity in these regions. The first one is related to scattering of s electrons on magnetic moments distributed in interphase boundaries that play the role of magnetic defects. Their contribution is unlikely to be large since $Dy_3Ru_4Al_{12}$ displays a strong magnetic anisotropy making domain walls quite narrow. As a result, they should occupy a small volume fraction in the sample and give a small contribution to the electrical resistivity.

A more likely reason for a large positive $\Delta\rho/\rho$ effect is different conduction electron spectra in phases with different magnetic structures [49]. The difference in the s-f interaction in different magnetic phases can give rise to a potential barrier at the boundary between phases. The projections of the Fermi surfaces at the interphase boundary plane cannot be fully overlapped in such cases, which should lead to the reflections of a part of the conduction electrons from a potential barrier at the interphase boundary and to the appearance of the additional $\Delta\rho/\rho$ peaks. The maximal $\Delta\rho/\rho$ value should correspond to the maximal number of states when conduction electrons are reflected from phase boundaries. Therefore, we can conclude that this number is higher when the magnetoresistance of $Dy_3Ru_4Al_{12}$ is measured in the transverse geometry than in the longitudinal. The anisotropy in the $\Delta\rho/\rho$ behavior in the intermediate state can be caused by a different orientation between the current direction and interphase boundaries and also by anisotropy of the Fermi surface. Pronounced peaks of the magnetoresistance were observed at the metamagnetic transitions in $ErGa_2$ [49], Tb_3Co [49], Dy_3Co [50], and in some $RNiGe_3$ compounds [51] in the field intervals where phases with different magnetic structure coexist.

A strong dependence of the magnetoresistance behavior on the relative orientation of magnetic field, electric current, and crystal axes in $Dy_3Ru_4Al_{12}$ is clearly seen from Figs. 11(e) and 11(f) which display the $\Delta\rho/\rho(H)$ dependencies measured in a magnetic field applied along the [001] axis with the current directed along the [100] and [001] axes, respectively. The magnetoresistance curve measured in the transversal geometry ($I \parallel [100]$, $H \parallel [001]$) shows a sharp peak which corresponds

to an intermediate state where a ferrimagneticlike phase and a noncollinear ferromagneticlike phase coexist, while in the longitudinal geometry, the $\Delta\rho/\rho$ peak in the same field interval is not observed. It should be noted that the peaks in $\Delta\rho/\rho$ measured in the transversal geometry [Fig. 11(e)] have different heights in the intermediate state in ascending and descending fields. It can be explained by differences in the domain structure of the sample, in particular, by different domain size, number, and orientation of interphase boundaries from which conduction electrons are reflected.

IV. DISCUSSION AND CONCLUSIONS

In the hexagonal crystal structure of the $Dy_3Ru_4Al_{12}$ compound, the Dy atoms are accommodated in distorted kagome nets. Although such a structure favors geometrical frustration, $Dy_3Ru_4Al_{12}$ displays long-range magnetic order due to additional contributions to the total free energy present in the system. Nevertheless, some distinctive features of frustration are evident. The origin of the complex electronic properties of $Dy_3Ru_4Al_{12}$ either lies directly in the $4f$ electronic shells or involves specific interactions which involve these shells.

The exchange interactions among various Dy^{3+} ions in $Dy_3Ru_4Al_{12}$ are of the Ruderman-Kittel-Kasuya-Yosida (RKKY) type and have an oscillatory long-ranged character. Different Dy atoms are involved in the exchange interactions to different extents since they reside on distorted kagome lattices. Another important contribution to the system's free energy comes from the electrostatic interaction between the crystalline electric field and the anisotropic $4f$ electronic orbitals of Dy. The magnetic structure is the result of a compromise between the exchange interactions and the crystal-field-induced anisotropy [8,52].

In an applied magnetic field, the total free energy includes an additional contribution, the Zeeman energy. As the magnetic field increases, the energy minimum corresponds to a different magnetic structure, which is reflected in field-induced rotations of magnetic moments. In this situation, the geometrical frustration plays the principal role in defining the magnetic structure of the compound. The field-induced magnetic phases cannot be considered as simple ferromagnetic since their magnetization is not equal to the forced ferromagnetic saturation, $30\mu_B$/f.u. The magnetoresistance study strongly supports this assumption and suggests the existence of incommensurate magnetic structures in the external field.

$Dy_3Ru_4Al_{12}$ exhibits strong interactions between the localized $4f$ electrons and the electrons that participate in the formation of conduction bands. This is evidenced by (i) the induction of spin fluctuations in the Ru $4d$ subsystem and (ii) the existence of a potential barrier at interphase boundaries for s electrons in applied magnetic field. The former is reflected in the strongly enhanced electronic effective mass, while the latter leads to the large positive magnetoresistance.

Further, the question of the order of the phase transition at the Néel temperature should be addressed. The sharp symmetrical peak in the specific heat [Fig. 9(a)] and the discontinuous change in the electrical resistivity (Fig. 10) imply that the order-disorder transition in $Dy_3Ru_4Al_{12}$ is of first order. Very similar variations of $C_p(T)$ and $R(T)$ were observed at the first-order transition in, e.g., $ErCo_2$ [53]. Further evidence can be obtained from the temperature dependence of the intensity of the magnetic reflection $(5/2\ -5/2\ 1/2)$ of $Dy_3Ru_4Al_{12}$ (Fig. 7). The intensity falls down steeply at $T = T_N$, which can be considered a discontinuous change in the order parameter. The temperature evolution of other magnetic reflections was studied as well and found to behave similarly. By contrast, in the case of a second-order phase transition at $T = T_N$ one would expect to observe a λ-type anomaly in C_p and a smoother change of the electrical resistivity and magnetic intensity. It is known that the PPMS device used for C_p measurements might not provide the adequate shape of C_p through first-order phase transitions since it does not account for the latent heat [54]. However, the temperature-time relaxation curve [Fig. 9(b)] displays arrests (shaded areas) on both the cooling and heating intervals, due to the latent heat at the phase transition. Thus, the raw specific heat data yield a conclusive proof of the first-order transition at T_N of $Dy_3Ru_4Al_{12}$.

Using the results obtained in the present work, one may provide an alternative interpretation of some electronic properties of $U_3Ru_4Al_{12}$ and analyze those unexplained in Ref. [20]. The relatively weak magnetic anisotropy, unexpected for a uranium intermetallic compound, requires a magnetization study in fields above 5 T used in Ref. [20]. The complex magnetic structure of $U_3Ru_4Al_{12}$ may provide a hint for a nontrivial behavior of the magnetization as a function of field, and field-induced transitions may be expected from the initial antiferromagnetic towards the forced ferromagnetic state.

The high $\gamma(0) \approx 600$ mJ mol^{-1} K^{-2} found for $U_3Ru_4Al_{12}$, comparable with $\gamma(0) \approx 500$ mJ mol^{-1} K^{-2} for $Dy_3Ru_4Al_{12}$, may originate from the polarization of the Ru $4d$ electronic states by the exchange field acting from the U $5f$ electrons. This is supported by the fact that the $5f$ electrons are to a great extent localized in $U_3Ru_4Al_{12}$, which follows from the high magnetic moment per U atom, 2.5 μ_B.

Additionally, $U_3Ru_4Al_{12}$ and $Dy_3Ru_4Al_{12}$ display different behaviors of the magnetoresistance. While for $Dy_3Ru_4Al_{12}$ $\Delta\rho/\rho > 0$ in both longitudinal and transverse geometries, for $U_3Ru_4Al_{12}$ in the transverse geometry the sign of $\Delta\rho/\rho$ depends on the direction of current flow: $\Delta\rho/\rho < 0$ for $I \parallel [100]$ and $\Delta\rho/\rho > 0$ for $I \parallel [001]$. In Ref. [20] this is explained by the existence of a spin density wave. Although this is a possible reason, an additional interpretation should be considered, namely, that magnetic field changes the periodicity of the magnetic structure in the opposite way along the basal plane and the hexagonal axis. Moreover, the interaction of the conduction electrons with the $5f$ magnetic moments should not be ignored in view of the results obtained for $Dy_3Ru_4Al_{12}$. Last but not least, the largest absolute magnetoresistance effect attained in fields up to 8 T is about 10% for $U_3Ru_4Al_{12}$, whereas for $Dy_3Ru_4Al_{12}$ it is more than by an order of magnitude higher.

While this discussion explains qualitatively some physical properties of $U_3Ru_4Al_{12}$, the issue of the orientation of the U magnetic moments outlined in the Introduction requires more experimental and probably theoretical work.

In conclusion, magnetic, thermal, and transport properties of a kagome lattice antiferromagnet $Dy_3Ru_4Al_{12}$ ($T_N = 7$ K) have been studied. A complex balance between the RKKY exchange interactions and the crystal-field-induced magnetic anisotropy results in a noncollinear magnetic structure with a propagation vector $(1/2\ 0\ 1/2)$. The antiferromagnetic-

paramagnetic phase transition is of first order as indicated by the anomalies in the specific heat and resistivity as well as by the rapid fall in the intensity of magnetic reflections at $T = T_N$. Despite the localized Dy magnetism, a strongly enhanced γ coefficient in the low-temperature specific heat, 500 mJ mol^{-1} K^{-2}, has been found. This might be explained by the presence of spin fluctuations induced in the Ru 4*d* subsystem by the *f*-*d* exchange. Along the principal crystallographic directions of $Dy_3Ru_4Al_{12}$ magnetization jumps have been found. Changes in the magnetic structure at the jumps affect the conduction electron spectra and are accompanied by large positive magnetoresistance.

ACKNOWLEDGMENTS

The work was performed in MLTL (http://mltl.eu/), which is supported within the program of Czech Research Infrastructures (Project No. LM2011025). It was supported by Czech Science Foundation (Grants No. P204/12/0150 and No. 14-03276S) and Czech Academy of Sciences (Project No. M10010203). The neutron diffraction experiment at LLB was supported by the European Commission through the Access Activities of the Integrated Infrastructure Initiative for Neutron Scattering and Muon Spectroscopy (NMI3), supported by the European Commission under the 7th Framework Programme through the Key Action: Strengthening the European Research Area, Research Infrastructures, Contract No. NMI3-II/FP7 283883. We acknowledge the support of HLD at HZDR, member of the European Magnetic Field Laboratory (EMFL). D.I.G. also acknowledges Charles University Grants No. SVV-2014-260091 and No. GAUK-703912. M.S.H. acknowledges the support of the Portuguese Foundation for Science and Technology through Grant No. SFRH/BD/66161/2009.

[1] R. Moessner and J. T. Chalker, Phys. Rev. B **58**, 12049 (1998).
[2] A. P. Ramirez, G. P. Espinosa, and A. S. Cooper, Phys. Rev. Lett. **64**, 2070 (1990).
[3] A. P. Ramirez, G. P. Espinosa, and A. S. Cooper, Phys. Rev. B **45**, 2505 (1992).
[4] G.-W. Chern and R. Moessner, Phys. Rev. Lett. **110**, 077201 (2013).
[5] J. N. Reimers, J. E. Greedan, and M. Bjorgvinsson, Phys. Rev. B **45**, 7295 (1992).
[6] M. J. P. Gingras, C. V. Stager, N. P. Raju, B. D. Gaulin, and J. E. Greedan, Phys. Rev. Lett. **78**, 947 (1997).
[7] R. Moessner and J. T. Chalker, Phys. Rev. Lett. **80**, 2929 (1998).
[8] D. Gignoux and D. Schmitt, J. Alloys Compd. **326**, 143 (2001).
[9] H. Maletta and V. Sechovský, J. Alloys Compd. **207-208**, 254 (1994).
[10] G. Ehlers and H. Maletta, Z. Phys. B **99**, 145 (1995).
[11] G. Ehlers, C. Ritter, A. Krutjakow, W. Miekeley, N. Stüßer, Th. Zeiske, and H. Maletta, Phys. Rev. B **59**, 8821 (1999).
[12] G. Ehlers, C. Ritter, J. R. Stewart, A. D. Hillier, and H. Maletta, Phys. Rev. B **75**, 024420 (2007).
[13] A. Dönni, G. Ehlers, H. Maletta, P. Fischer, H. Kitazawa, and M. Zolliker, J. Phys.: Condens. Matter **8**, 11213 (1996).
[14] P. Javorský, P. Burlet, E. Ressouche, V. Sechovský, and G. Lapertot, J. Magn. Magn. Mater. **159**, 324 (1996).
[15] P. Javorský, P. Burlet, E. Ressouche, V. Sechovský, H. Michor, and G. Lapertot, Physica B **225**, 230 (1996).
[16] A. P. Gonçalves, A. P. Waerenborgh, P. Gaczyński, H. Noël, and O. Tougait, Intermetallics **17**, 25 (2009).
[17] O. Tougait, H. Noël, and R. Troć, J. Solid State Chem. **177**, 2053 (2004).
[18] O. Tougait, R. Troć, A. Zaleski, and H. Noël, Philos. Mag. **87**, 1085 (2007).
[19] M. Pasturel, O. Tougait, M. Potel, T. Roisnel, K. Wochowski, H. Noël, and R. Troć, J. Phys.: Condens. Matter **21**, 125401 (2009).
[20] R. Troć, M. Pasturel, O. Tougait, A. P. Sazonov, A. Gukasov, C. Sułkowski, and H. Noël, Phys. Rev. B **85**, 064412 (2012).
[21] W. Ge, H. Ohta, Ch. Michioka, and K. Yoshimura, J. Phys.: Conf. Ser. **344**, 012023 (2012).
[22] S. Nakamura, S. Toyoshima, N. Kabeya, K. Katoh, T. Nojima, and A. Ochiai, JPS Conf. Proc. **3**, 014004 (2014).
[23] M. D. Kuz'min and A. M. Tishin in *Handbook of Magnetic Materials*, edited by K. H. J. Buschow (Elsevier, Amsterdam, 2008), Vol. 17, p. 149.
[24] See http://www.ill.eu/sites/fullprof/.
[25] R. E. Gladyshevskii, O. R. Strusievicz, K. Cenzual, and E. Parthé, Acta Crystallogr. B **49**, 474 (1993).
[26] J. Niermann and W. Jeitschko, Z. Anorg. Allg. Chem. **628**, 2549 (2002).
[27] N. G. Bukhan'ko, A. I. Tursina, S. V. Malyshev, A. V. Gribanov, Yu. D. Seropegin, and O. I. Bodak, J. Alloys Compd. **367**, 149 (2004).
[28] Y. Skourski, M. D. Kuz'min, K. P. Skokov, A. V. Andreev, and J. Wosnitza, Phys. Rev. B **83**, 214420 (2011).
[29] A. Gukasov, A. Goujon, J.-L. Meuriot, Ch. Person, G. Exil, and G. Koskas, Physica B **397**, 131 (2007).
[30] V. Petříček, M. Dušek, and L. Palatinus, JANA2006, Structure Determination Software Programs, Institute of Physics, Praha, Czech Republic, 2008.
[31] R. W. Hill and K. A. Gschneidner, Jr., J. Phys. F: Met. Phys. **18**, 2545 (1988).
[32] T.-W. E. Tsang, K. A. Gschneidner, Jr., F. A. Schmidt, and D. K. Thome, Phys. Rev. B **31**, 235 (1985).
[33] I. A. Campbell, J. Phys. F: Met. Phys. **2**, L47 (1972).
[34] N. V. Baranov, K. Inoue, H. Michor, G. Hilscher, and A. A. Yermakov, J. Phys.: Condens. Matter **15**, 531 (2003).
[35] N. V. Baranov, H. Michor, G. Hilscher, A. Proshkin, and A. Podlesnyak, J. Phys.: Condens. Matter **20**, 325233 (2008).
[36] S. C. Abrahams, J. L. Bernstein, R. C. Sherwood, J. H. Wernick, and H. J. Williams, J. Phys. Chem. Solids **25**, 1069 (1964).
[37] M. Cyrot and M. Lavagna, J. Phys. (France) **40**, 763 (1979).
[38] E. Talik, M. Neumann, A. Ślebarski, and A. Winiarski, Physica B **212**, 25 (1995).
[39] K. Yano, I. Umehara, K. Sato, and A. Yaresko, Solid State Commun. **136**, 67 (2005).
[40] M. Mizumaki, K. Yano, I. Umehara, F. Ishikawa, K. Sato, A. Koizumi, N. Sakai, and T. Muro, Phys. Rev. B **67**, 132404 (2003).

[41] K. Yano, Y. Tanaka, I. Matsumoto, I. Umehara, K. Sato, H. Adachi, and H. Kawata, J. Phys.: Condens. Matter **18**, 6891 (2006).
[42] N. F. Mott and H. Jones, *The Theory of the Properties of Metals and Alloys* (Oxford University Press, New York, 1958).
[43] P. E. Markin and N. V. Baranov, J. Alloys Compd. **228**, 54 (1995).
[44] S. N. Jammalamadaka, N. Mohapatra, S. D. Das, and E. V. Sampathkumaran, Phys. Rev. B **79**, 060403(R) (2009).
[45] N. Mohapatra, K. Mukherjee, K. K. Iyer, and E. V. Sampathkumaran, J. Phys: Condens. Matter **23**, 496001 (2011).
[46] R. J. Elliott and F. A. Wedgwood, Proc. Phys. Soc. London **81**, 846 (1963).
[47] D. Gignoux and D. Schmitt, Phys. Rev. B **48**, 12682 (1993).
[48] E. Yi Chen, J. F. Dillon, Jr., and H. J. Guggenheim, J. Appl. Phys. **48**, 804 (1977).
[49] N. V. Baranov, P. E. Markin, A. I. Kozlov, and E. V. Sinitsyn, J. Alloys Compd. **200**, 43 (1993).
[50] N. V. Baranov, E. Bauer, R. Hauser, A. Calatanu, Y. Aoki, and H. Sato, Eur. Phys. J. B **16**, 67 (2000).
[51] E. D. Mun, S. L. Bud'ko, H. Kob, G. J. Miller, and P. C. Canfield, J. Magn. Magn. Mater. **322**, 3527 (2010).
[52] A. P. Ramirez, in *Handbook of Magnetic Materials*, edited by K. H. J. Buschow (Elsevier, Amsterdam, 2001), Vol. 13, p. 423.
[53] N. H. Duc, T. D. Hien, P. E. Brommer, and J. J. M. Franse, J. Phys. F: Met. Phys. **18**, 275 (1988).
[54] J. C. Lashley, M. F. Hundley, A. Migliori, J. L. Sarrao, P. G. Pagliuso, T. W. Darling, M. Jaime, J. C. Cooley, W. L. Hults, L. Morales, D. J. Thoma, J. L. Smith, J. Boerio-Goates, B. F. Woodfield, G. R. Stewart, R. A. Fisher, and N. E. Phillips, Cryogenics **43**, 369 (2003).